



Contents lists available at ScienceDirect

Journal of Structural Biology

journal homepage: [www.elsevier.com/locate/yjsbi](http://www.elsevier.com/locate/yjsbi)

## Technical Note

## Graphene: Substrate preparation and introduction

Radosav S. Pantelic<sup>a</sup>, Ji Won Suk<sup>b</sup>, Carl W. Magnuson<sup>b</sup>, Jannik C. Meyer<sup>c</sup>, Philipp Wachsmuth<sup>c</sup>, Ute Kaiser<sup>c</sup>, Rodney S. Ruoff<sup>b</sup>, Henning Stahlberg<sup>a,\*</sup><sup>a</sup> Center for Cellular Imaging and Nano Analytics, Biozentrum, University of Basel, Basel, Switzerland<sup>b</sup> Department of Mechanical Engineering and The Texas Materials Institute, University of Texas, Austin, TX, USA<sup>c</sup> Electron Microscopy Department of Materials Sciences, University of Ulm, Ulm, Germany

## ARTICLE INFO

## Article history:

Received 4 August 2010

Received in revised form 29 September 2010

Accepted 4 October 2010

Available online xxxxx

## Keywords:

Graphene

Graphene oxide

Cryo-EM

Electron microscopy

DNA

Transmission electron microscopy

## ABSTRACT

This technical note describes the transfer of continuous, single-layer, pristine graphene to standard Quantifoil TEM grids. We compare the transmission properties of pristine graphene substrates to those of graphene oxide and thin amorphous carbon substrates. Positively stained DNA imaged across amorphous carbon is typically indiscernible and requires metal shadowing for sufficient contrast. However, in a practical illustration of the new substrates properties, positively stained DNA is imaged across pristine graphene in striking contrast without the need of metal shadowing. We go onto discuss technical considerations and the potential applications of pristine graphene substrates as well as their ongoing development.

© 2010 Elsevier Inc. All rights reserved.

## 1. Introduction

Despite the benefits of highly transparent crystalline substrates being long since recognized, technical difficulties with their preparation have prevented wide scale application (Dobelle and Beer, 1968; Hahn and Baumeister, 1974). Recent developments in the large scale synthesis of pristine graphene (Li et al., 2009c) present interesting possibilities for structural techniques that up until now have required amorphous carbon substrates (e.g. 2D electron crystallography and new emerging methods (Benesch et al., submitted for publication; Kelly et al., 2008; Rhinow and Kühlbrandt, 2008)).

Crystalline substrates are effectively transparent to transmission electron microscopy (TEM) at resolutions below their periodicity, and at higher resolutions the periodic nature of the signal facilitates subtraction if necessary (Meyer et al., 2008a). At crystalline periodicities of 2.13 and 1.23 Å, respectively (Meyer et al., 2007), structural details of pristine graphene are outside the resolutions typically resolved in biological TEM. At a single layer thickness of 0.34 nm (Eda et al., 2008), the minimal scattering cross-section of pristine graphene also minimizes background (noise) contributed by inelastic and multiple scattering within the substrate. Other remarkable properties are also derived from the highly ordered structure of graphene, including high mechanical

strength/elasticity (Lee et al., 2008; Wang et al., 2009a; Zakharchenko et al., 2009) and “ballistic” electrical conductivity, also at liquid nitrogen temperatures (Heersche et al., 2007; Zhang et al., 2005). Although the threshold for knock-on damage is ~86 keV (Zobelli et al., 2007), we have found graphene substrates to be remarkably stable, withstanding acceleration voltages of up to 300 keV under the typically lower electron dose conditions (as little as 20–30 e/Å<sup>2</sup>) of biological TEM. The electrical conductivity of graphene, converted into bulk units and assuming a thickness of 3.4 Å, is more than six orders of magnitude higher than that of amorphous carbon (Chen et al., 2008; Robertson, 1986; Ziegler, 2006). Hence, graphene substrates may potentially reduce the effects of charging and improve the imaging stability of insulating materials like amorphous ice.

In previous work we introduced the use of graphene oxide (GO), a hydrophilic derivative of pristine graphene with semi-crystalline properties (Pantelic et al., 2010). Surface bound, oxidized functional groups contribute to the hydrophilic properties of the substrate, but also introduce a weak background signal. Oxidation also increases the thickness of pristine graphene to ~1 nm (Stankovich et al., 2006; Wang et al., 2009b), consequently increasing inelastic scattering within the substrate and introducing additional background noise. But in particular, deposition from solution produces substrates composed of overlapped/stacked platelets that are thus inhomogeneous.

Chemical vapor deposition (CVD) is a method of chemically producing continuous areas of pristine monolayer (>95%, and recently

\* Corresponding author. Fax: +41 61 387 39 86.

E-mail address: [Henning.Stahlberg@unibas.ch](mailto:Henning.Stahlberg@unibas.ch) (H. Stahlberg).

completely monolayer (Li et al., 2009a,b)) graphene across thin Cu foils of any size (Li et al., 2009c; Yu et al., 2008). From these Cu foils, the graphene is directly transferrable to standard Quantifoil TEM grids by evaporation of solvent (to adhere the graphene) followed by chemical wet etching (to dissolve the Cu foil). This technical note discusses a method by which graphene is transferred and compares the substrate to previous graphene oxide and amorphous carbon substrates. The high transparency of the substrate is illustrated by an example in which positively stained double-stranded DNA is imaged in high contrast, without the necessity of metal shadowing.

## 2. Transfer and preparation of the substrate

Graphene is prepared by CVD across thin Cu foils according to previous work (Li et al., 2009c). Following CVD, monolayer graphene covers both sides of a 25- $\mu\text{m}$  thick Cu foil. For single layer transfer, one side of the foil must be pre-etched by floating across 10%  $\text{Fe}(\text{NO}_3)_3$  aqueous solution for  $\sim 30$ – $40$  min, after which the graphene on the lower side of the foil can be rinsed away in water. The now single-sided foil is cleaned in 10% HCl solution for  $\sim 10$  min to remove contaminants bound to the graphene. Quantifoil 200 mesh gold (highly flexible and resistant to copper etching) TEM grids (Quantifoil Micro Tools GmbH, Jena, Germany) are plasma cleaned for 30 s (to improve adhesion to the graphene) and placed across the Cu foil with the carbon side in direct contact with the graphene. Small droplets of chloroform are placed across the foil, spreading and saturating the space between the Quantifoil and graphene. As the chloroform evaporates, the carbon of the Quantifoil grids is pulled into close contact with the graphene where it is strongly held in place (Meyer et al., 2008b).

Chloroform is preferable as an adhesion promoter, given its purity, and any incidental moisture can easily be seen floating across the surface of the saturated area. Once dry, heating at  $200^\circ\text{C}$  (in air) for  $\sim 15$  min also improves adhesion of the grids by evaporating any trapped moisture, but the temperature should be raised slowly to avoid any boiling that may dislodge the grids. Once cooled to room temperature, formvar plastic (0.5% concentration) is coated across the attached grids, stabilizing them and promoting a gradual etching of the copper from one side. It is important that the formvar is coated only on one side, otherwise insufficient circulation during etching leaves remnant trace copper and contaminants. After  $\sim 36$  h etching in  $\text{Fe}(\text{NO}_3)_3$  aqueous solution (2.5 wt.% concentration, mildly agitated during etching by a mixer), only the graphene remains bound to the Quantifoil grids. After thorough rinsing in water, the formvar backing is dissolved in chloroform.

With delicate handling and use of thin, flat Cu foils and TEM grids, the transfer of monolayer graphene is consistent and reproducible. The only concern is minimizing precipitates and contamination left by wet etching of the copper. Pre-filtering of etching solutions through a  $0.2\ \mu\text{m}$  PTFE membrane minimizes coarse precipitates that tend to accumulate across the graphene. Cleaning of transferred grids in HCl (minimum 7 vol.% concentration) for approximately 2–4 h further removes any traces of etching solution and contamination otherwise bound to the graphene surface.

## 3. Comparison of substrates

The term “pristine” is somewhat subjective since substrates may be free of bulk amorphous material and demonstrate high transparency, but may nonetheless fail to be *atomically* pristine (additional adsorbates bound to the surface of the graphene). For full transparency, substrates are baked in high vacuum at temperatures  $>300^\circ\text{C}$ , beyond which stable groups bound to the graphene surface are gradually released (Paredes et al., 2008; Zhang et al.,

2009). Fig. 1 compares signal from separate images of monolayer pristine graphene (Fig. 1; green,  $\sim 400^\circ\text{C}$  vacuum heated), graphene oxide (Fig. 1; black, prepared according to (Pantelic et al., 2010)), and thin amorphous carbon (Fig. 1; red) samples. Power spectra were calculated from images taken at  $145,000\times$  magnification ( $0.87\ \text{\AA}$  unbinned image pixel size) at  $\sim 200$  nm defocus. Data were collected to pre-GIF CCD camera (1s exposure time, Gatan MSC742  $1024 \times 1024$  pixel,  $24\ \mu\text{m}$  physical pixel size) using a FEI Titan low-base TEM equipped with image spherical aberration corrector (spherical aberration  $C_s = 0$  mm,  $\pm 2\ \mu\text{m}$ ) and Gatan TriDiem, operated at 80 keV. Beam intensity was kept to a nominal count of  $\sim 10^4$  electrons per pixel.

Compared to amorphous carbon, graphene oxide demonstrates an approximate 40% reduction in phase contrast (note the logarithmic scale) and complete reduction/cancellation of signal up to  $0.35\ \text{\AA}^{-1}$  (opposed to carbon reaching  $0.42\ \text{\AA}^{-1}$ ). However, in absence of amorphous oxidation, pristine graphene demonstrates no phase contrast component other than the first reflection at  $2.13\ \text{\AA}$ . The first crystalline reflection also appears sharper in the pristine graphene sample compared to the graphene oxide, which sustains many crystal defects from the harsh oxidization process. In fact, the only signal imposed by pristine crystalline substrates below their periodicity is amplitude contrast/background primarily from inelastic scattering within the substrate.

Pristine monolayer graphene ( $\sim 0.34$  nm thickness) demonstrates a minimal background (baseline) up to one order of magnitude less than the amorphous carbon sample, with monolayer graphene oxide closely comparable (Fig. 1; green and black curves). The minimal background imposed by the pristine graphene substrate is further emphasized by comparison to a power spectral curve calculated from an empty frame (vacuum, void of any sample scattering) exposed under the same electron dose per pixel (Fig. 1; magenta). The reduced inelastic cross-section of the pristine graphene sample minimizes inelastic scattering within the substrate thus reducing background, as confirmed by EELS. Fig. 2 compares the inelastic energy loss of graphene oxide (Fig. 2; black) and pristine graphene (Fig. 2; green) samples at 1 and 3 layers

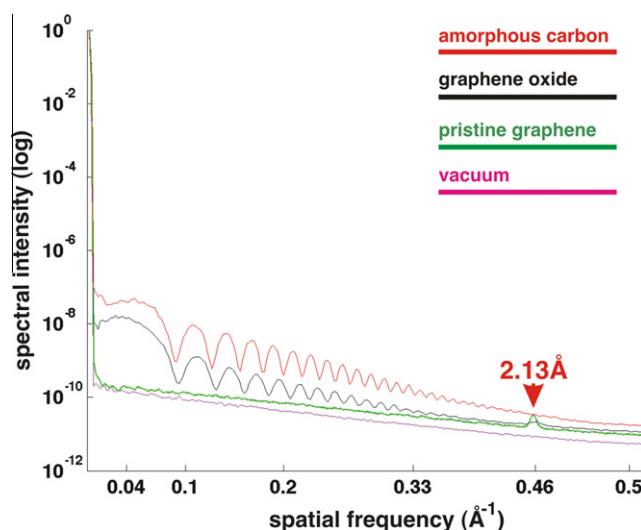


**Fig. 1.** Comparison of introduced substrate signal by power spectra: a comparison of power spectral densities calculated from images (collected at  $\sim 200$  nm defocus and  $145,000\times$  magnification) of thin amorphous carbon (red,  $\sim 3$ – $4$  nm thickness as determined by Quartz crystal meter), monolayer graphene oxide (black,  $\sim 1$  nm thickness, heated at  $\sim 300^\circ\text{C}$  in air to partially reduce oxidization and optimize transmission properties (Pantelic et al., 2010)) and monolayer pristine graphene (green,  $\sim 0.34$  nm thickness, annealed to pristine at  $400^\circ\text{C}$  in vacuum) substrates. The magenta curve is calculated from an empty frame (vacuum, exposed with the same nominal count of  $\sim 10^4$  electrons per pixel) and provides a baseline by which the transparency of the pristine graphene sample can be further appreciated.

(Fig. 2a and b, respectively, found by surveying different areas of the grid) to thin amorphous carbon (Fig. 2; red). Multiple spectra collected at 0.4 s exposure time and energy dispersion of 0.1 eV/pixel (using a 30  $\mu\text{m}$  objective aperture) were aligned and averaged for each sample. A 2.0 mm GIF aperture was tuned for an average zero-loss peak width of 0.645–0.68 eV.

At up to three layers thickness the pristine graphene sample maintains a discrete peak with minimal loss at lower energies, mainly due to the reduced thickness of the sample. Although also demonstrating significantly reduced inelastic loss, the semi-amorphous graphene oxide sample yields a broader/higher mean energy loss that increases by an order of at least two with additional layers (Fig. 2b; black). This increase is not necessarily linear given the inhomogeneous oxidization of individual graphene oxide layers. The increased scattering by *monolayer* graphene oxide may perhaps be considered not so significant. However, the accumulation of amorphous bulk with each oxidized layer diminishes the benefits of the substrate rapidly with more layers – a particularly pertinent consideration given the in-homogeneity of graphene oxide substrates deposited from solution.

Upon exposure to air, the pristine graphene gradually becomes interspersed with sparsely accumulated adsorbates that begin to attenuate transmission properties. After  $\sim 90$  min ambient exposure (at room temperature) the samples nonetheless remain

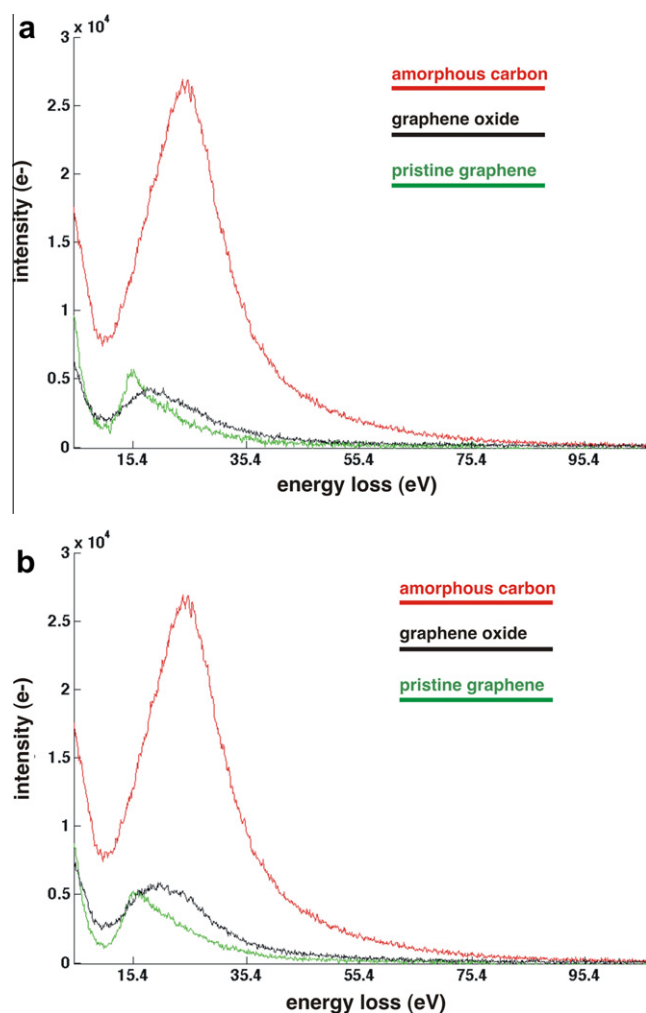


**Fig. 2.** Comparison of inelastic scattering by EELS: the reduced baseline/background component (noise) demonstrated by either graphene-based sample is attributed to reduced inelastic scattering cross-sections, as confirmed by EELS. The energy loss within amorphous carbon (red), graphene oxide (black), and graphene (green) at monolayer (a) and three layers (b) are compared.

largely near-pristine (Fig. 3; green) as adsorbates initially tend to localize around sparse defects within the graphene structure. Interestingly, the areas most degraded by amorphous accumulation (Fig. 3; blue) still demonstrate a reduction in phase contrast compared to graphene oxide beyond  $0.17 \text{ \AA}^{-1}$  (Fig. 3; black). Hence, exposure/handling of substrates within reasonable limits during sample preparation should not yield significant attenuation of the pristine substrates transmission properties.

#### 4. A practical illustration of substrate transparency using positively stained DNA

Due to the relative simplicity and effectiveness, DNA samples are still often prepared at room temperature across amorphous carbon substrates. However, the particularly poor contrast of uncoiled DNA across amorphous carbon necessitates the use of metal shadowing techniques. Hence, in a practical illustration of the background properties of pristine graphene, we sought to image DNA without metal shadowing.

Plasmid DNA of pSK-CIC-ec1, encoding for the *Escherichia coli* chloride proton antiporter (CIC) is a double stranded plasmid of approximately 7 Kbp and was a generous gift from the Joseph Mindehl group (NIH). The plasmid was prepared for imaging according to a protein-free spreading technique (Bratosin-Guttman, 1992). A 20  $\mu\text{l}$  aliquot of plasmid DNA at a concentration of  $\sim 5 \mu\text{g/ml}$  was diluted in 30  $\mu\text{l}$  of ammonium acetate (0.25 M concentration), then left to incubate for approximately 1 min. Used to promote spreading, 1.25  $\mu\text{l}$  of Tris (dimethylaminomethyl) phenol (DMP-30, SPI #02823, SPI supplies, West Chester, USA) freshly diluted in distilled water to 2% concentration was then added. A droplet of the final solution was placed across a covered sterile Petri dish and left to incubate for  $\sim 30$  min. DNA spread by diffusion across a DMP monolayer formed at the air–water interface of the droplet was picked up with a graphene grid (pre-baked in vacuum at  $400^\circ\text{C}$  for  $\sim 35$  min) and immediately stained for 1 min with 1% uranyl acetate (diluted from 2% stock with 50% ethanol) before washing thoroughly in 50% ethanol by blotting and wetting repeatedly. The positively stained plasmid DNA was imaged at liquid nitrogen temperature in TEM brightfield mode using an FEI Titan KRIOS operated at 80 keV. Data were recorded at  $37,000\times$  magnification with 2-fold binning for a final image pixel size of  $4.4 \text{ \AA}$  using a

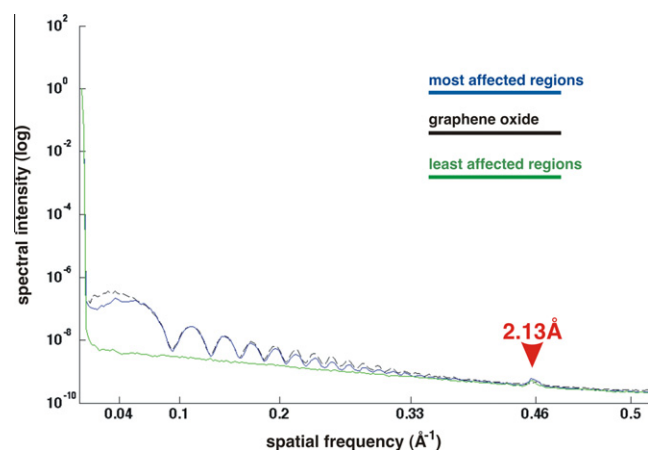


**Fig. 3.** Effects of exposure and consequent attenuation of signal: a comparison of signal calculated from images ( $145,000\times$  nominal magnification and  $\sim 200$  nm defocus) of monolayer graphene oxide (black) and different areas of an exposed monolayer pristine graphene sample are presented (green, blue). The exposed graphene sample remains largely near pristine as demonstrated by a representative region (green). The blue curve is representative of localized regions most affected by the amorphous accumulation of adsorbates.

Gatan Ultrascan 4000 CCD camera (4096 × 4096 pixel, 15 μm physical pixel size) at 2 s exposure time.

Fig. 4 shows positively stained relaxed circular plasmid DNA spread across pristine graphene, in strong contrast despite the absence of metal shadowing. Given the high substrate transparency, buffer constituents contribute more to background than they would across thicker substrates. Although one may expect a completely “transparent” background, in this example the majority of apparent background is likely the bound DMP-30 that is now more apparent given the transparency of the substrate. Such an application of pristine graphene to the imaging of positively stained DNA in high contrast without the necessity of metal shadowing serves well as a practical illustration of the substrates high transparency.

## 5. Conclusion

With further development we anticipate numerous applications of CVD graphene substrates to a wide variety of samples and

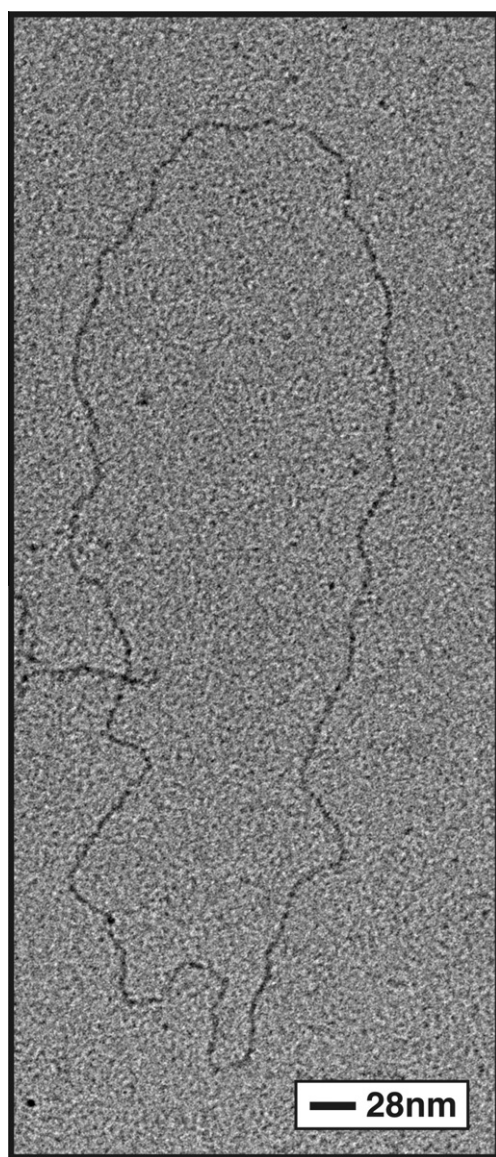


**Fig. 4.** Application of graphene substrates to the imaging of DNA: given the high transparency of graphene, relaxed circular plasmid DNA is discernable with particularly strong contrast (brightfield TEM, 37,000× nominal magnification and –2.5 μm defocus), without the necessity of metal shadowing or darkfield TEM. Rather than completely transparent, the minimal background present is likely the DMP-30 monolayer used to spread the DNA.

techniques where amorphous carbon has been previously required. As a purely crystalline substrate free from attenuation by oxidation (Pantelic et al., 2010), pristine graphene is transparent to TEM. However, in the absence of oxidation the substrate is inherently hydrophobic. In a practical illustration of the substrates high transparency, we have demonstrated the use of a DMP-30 monolayer in the imaging of DNA across graphene without the necessity of metal shadowing. As a hydrophobic substrate *pristine* graphene may also be currently suited to other monolayer-based approaches (Kelly et al., 2008) and hydrophobic molecules.

The direct transfer of pristine graphene from CVD foils produces a *continuous, monolayer* (0.34 nm) substrate covering approximately 90% of a Quantifoil grid. Hence, unlike graphene oxide substrates deposited from solution, CVD transferred substrates are much thinner and homogenous in thickness. Wider applications of this substrate will be feasible once suitable hydrophobic treatments are developed. Traditional glow discharging/plasma cleaning methods are limited as the highly thin graphene substrates suffer direct knock-on damage/etching (consequently attenuating the physical and transmission properties of the substrate, data not shown). The properties of graphene oxide are strongly attenuated by coarse and harsh chemical oxidation. However, an in situ treatment of pristine graphene substrates rendering them hydrophilic while minimizing attenuation of the graphene's inherent properties (i.e. a controlled, gentle chemical functionalization or gas annealing) should be feasible and preferable. The trial and development of such processes is the focus of ongoing work.

## Acknowledgments

We wish to acknowledge Prof. Dr. Wolfgang Baumeister and Dr. Jürgen Plitzko for their support during the preliminary stages of our research into graphene. We thank Drs. Shirley Müller, Phillippe Ringler, and Mohamed Chami for fruitful discussions, and Priyanka Abeyrathne and Paul Baumgartner for their help with preparation of DNA samples. Plasmid DNA of pSK-CIC-ec1 was a kind gift from the Joseph Mindell group (NIH). This work was in part supported by the Swiss National Science foundation (SystemsX.ch). The group of Prof. Rodney S. Ruoff appreciates support from the DARPA iMINT and DARPA CERA centres, the Office of Naval Research, and the Advanced Energy Consortium. The group of Prof. Ute Kaiser acknowledges the financial support provided by the German Research Foundation (DFG) and Ministry of Science, Research and Arts (MWK) of Baden-Württemberg state within the SALVE (Sub Angstrom Low-Voltage Electron Microscopy) project.

## References

- Benesch, L.P., Ruotolo, B.T., Simmons, D.A., Barrera, N.P., Morgner, N., Wang, L., Saibil, H.R., Robinson, C.V., 2009. Visualizing protein assemblies by means of preparative mass spectrometry and microscopy. *J. Struct. Biol.* submitted for publication.
- Bratosin-Guttman, S., 1992. A new method for the routine spreading of DNA in protein-free conditions. *Journal of Structural Biology* 108, 162–167.
- Chen, J.H., Jang, C., Adam, S., Fuhrer, M.S., Williams, E.D., Ishigami, M., 2008. Charged-impurity scattering in graphene. *Nature Physics* 4, 377–381.
- Dobelle, W.H., Beer, M., 1968. Chemically cleaved graphite support films for electron microscopy. *Journal of Cell Biology* 39, 733–735.
- Eda, G., Fanchini, G., Chowalla, M., 2008. Large-area ultrathin films of reduced graphene oxide as a transparent and flexible electronic material. *Nature Nanotechnology* 3, 270–274.
- Hahn, M., Baumeister, W., 1974. High resolution negative staining of ferritin molecules on vermiculite single crystal supports. *Biochimica et Biophysica Acta* 371, 267.
- Heersche, H.B., Jarillo-Herrero, P., Oostinga, J.B., Vandersypen, L.M.K., Morpurgo, A.F., 2007. Bipolar supercurrent in graphene. *Nature* 446, 56–59.
- Kelly, D.F., Dukovski, D., Walz, T., 2008. Monolayer purification: a rapid method for isolating protein complexes for single-particle electron microscopy. *Proceedings of the National Academy of Sciences* 105, 4703.
- Lee, C., Wei, X., Kysar, J.W., Hone, J., 2008. Measurement of the elastic properties and intrinsic strength of monolayer graphene. *Science* 321, 385.

- Li, X., Cai, W., Colombo, L., Ruoff, R., 2009a. Evolution of graphene growth on Ni and Cu by carbon isotope labeling. *Nano Letters* 9, 4268–4272.
- Li, X., Zhu, Y., Cai, W., Borysiak, M., Han, B., Chen, D., Piner, R., Colombo, L., Ruoff, R., 2009b. Transfer of large-area graphene films for high-performance transparent conductive electrodes. *Nano Letters* 9, 4359–4363.
- Li, X.S., Cai, W.W., An, J.H., Kim, S., Nah, J., Yang, D.X., Piner, R., Velamakanni, A., Jung, I., Tutuc, E., Banerjee, S.K., Colombo, L., Ruoff, R.S., 2009c. Large-area synthesis of high-quality and uniform graphene films on copper foils. *Science* 324, 1312–1314.
- Meyer, J.C., Girit, C.O., Crommie, M.F., Zettl, A., 2008a. Imaging and dynamics of light atoms and molecules on graphene. *Nature* 454, 319–322.
- Meyer, J.C., Girit, C.O., Crommie, M.F., Zettl, A., 2008b. Hydrocarbon lithography on graphene membranes. *Applied Physics Letters* 92, 123110.
- Meyer, J.C., Geim, A.K., Katsnelson, M.I., Novoselov, K.S., Booth, T.J., Roth, S., 2007. The structure of suspended graphene sheets. *Nature* 446, 60–63.
- Pantelic, R., Meyer, J., Kaiser, U., Baumeister, W., Pitzko, J., 2010. Graphene oxide: a substrate for optimizing preparations of frozen-hydrated samples. *Journal of Structural Biology* 170, 152–156.
- Paredes, J., Villar-Rodil, S., Martinez-Alonso, A., Tascon, J., 2008. Graphene oxide dispersions in organic solvents. *Langmuir* 24, 10560–10564.
- Rhinow, D., Kühlbrandt, W., 2008. Electron cryo-microscopy of biological specimens on conductive titanium–silicon metal glass films. *Ultramicroscopy* 108, 698–705.
- Robertson, J., 1986. Amorphous carbon. *Advances in Physics* 35, 317–374.
- Stankovich, S., Dikin, D.A., Dommett, G.H.B., Kohlhaas, K.M., Zimney, E.J., Stach, E.A., Piner, R.D., Nguyen, S.B.T., Ruoff, R.S., 2006. Graphene-based composite materials. *Nature* 442, 282–286.
- Wang, G.X., Shen, X.P., Wang, B., Yao, J., Park, J., 2009a. Synthesis and characterisation of hydrophilic and organophilic graphene nanosheets. *Carbon* 47, 1359–1364.
- Wang, G.X., Wang, B., Park, J., Yang, J., Shen, X.P., Yao, J., 2009b. Synthesis of enhanced hydrophilic and hydrophobic graphene oxide nanosheets by a solvothermal method. *Carbon* 47, 68–72.
- Yu, Q.K., Lian, J., Siriponglert, S., Li, H., Chen, Y.P., Pei, S.S., 2008. Graphene segregated on Ni surfaces and transferred to insulators. *Applied Physics Letters* 93, 113103.
- Zakharchenko, K.V., Katsnelson, M.I., Fasolino, A., 2009. Finite temperature lattice properties of graphene beyond the quasiharmonic approximation. *Physical Review Letters* 102, 046808.
- Zhang, X., Huang, Y., Wang, Y., Ma, Y., Liu, Z., Chen, Y., 2009. Synthesis and characterization of a graphene-C60 hybrid material. *Carbon* 47, 334–337.
- Zhang, Y., Tan, Y.W., Stormer, H.L., Kim, P., 2005. Experimental observation of the quantum Hall effect and Berry's phase in graphene. *Nature* 438, 201–204.
- Ziegler, K., 2006. Robust transport properties in graphene. *Physical Review Letters* 97, 266802.
- Zobelli, A., Gloter, A., Ewels, C., Seifert, G., Colliex, C., 2007. Electron knock-on cross section of carbon and boron nitride nanotubes. *Physical Review B* 75, 245402.